Available online at www.sciencedirect.com
ScienceDirect
Ceramics International 35 (2009) 961–966
CERAMICS INTERNATIONAL
www.elsevier.com/locate/ceramint

Tin oxide nanoparticles synthesized by gel combustion and their potential for gas detection

Huan Liu [a], Shuping Gong [a], Yunxiang Hu [a,b], Jun Zhao [a], Jianqiao Liu [a], Zhiping Zheng [a], Dongxiang Zhou [a,*]

[a] *Engineering Research Center for Functional Ceramics of the Ministry of Education, Department of Electronic Science & Technology, Huazhong University of Science & Technology, No. 1037 Luoyu Road, Hongshan District, Wuhan City 430074, PR China*
[b] *Ministry-of-Education Key Laboratory for the Synthesis and Application of Organic Functional Molecules, Hubei University, Wuhan City 430062, PR China*

Received 2 January 2008; received in revised form 1 February 2008; accepted 2 April 2008
Available online 11 July 2008

Abstract

Tin oxide nanoparticles were synthesized starting from $SnCl_4{\cdot}5H_2O$ with the aid of polyacrylamide gel. The pyrolysis of the gel and the influence of the calcination temperature were discussed based on thermogravimetric analysis and X-ray powder diffraction. The decomposition of the polyacrylamide gel occurred mainly in the temperature range of 220–600 °C, after which resulting in a heap of fine powders. The average grain size of the nanoparticles synthesized at 600, 700 and 800 °C were calculated to be 8.1, 19.2 and 27.9 nm, respectively. The prepared SnO_2 nanoparticles were sphere-like and uniform in size, weakly aggregated in thin platelets as indicated by scanning electron microscope (SEM) images. Thick-film sensor samples based on the as-synthesized SnO_2 nanoparticles without specific additives showed response sensitivity of around 28.8 at the optimal detection temperature of 150 °C to 30 ppm H_2S gas, while their responses to 1000 ppm of CO or CH_4 were negligible.

Keywords: Tin oxide; Nanoparticles; Polyacrylamide gel

1. Introduction

Semiconducting metal oxides in general and SnO_2 in particular, have been investigated extensively for the purpose of practical applications such as gas leak detecting and environmental monitoring. Yamazoe et al. [1,2] proposed that the process of gas sensing by metal-oxide sensor involves receptor function and transduction function. These results had a substantial impact on the designing of metal oxide gas sensors [3]. The biggest draw back of undoped SnO_2 gas sensor material is its low sensitivity and selectivity [4]. For example, the sensitivity of the undoped SnO_2 thick film toward 300 ppm of H_2S gas was 10 at the optimal operation temperature of 350 °C [5]. Therefore, noble metals such as Pt, Pd, Ru, Au and Ag or specific dopants for certain gas are intentionally introduced, promoting the receptor function and thus improving the sensitivity and selectivity [2]. On the other hand, findings of grain size effects [6,7] on the sensor response through the transducer function have made nanocrystalline semiconducting oxides very promising for gas detection [8,9]. Microstructure control of the sensing materials, especially the grain size and porosity, hence become fundamental for the enhancement of gas-sensing performance [10–12].

The method and condition of SnO_2 nanoparticles preparation are very important for the control of the microstructure of sensing bodies and thus expected to influence the electrical properties [13]. Both chemical and physical methods have been widely investigated, such as homogeneous precipitation [14], sol–gel method [15], hydrothermal method [16], Pechini route [17], laser ablation technique [18] and high-energy ball milling technique [19]. In fact, many authors proved that the sintering of nanoparticles under standard conditions used for micron-sized particles led to a dramatic growth of the particles and to a loss of the nanostructure in the sintered sample [20]. The synthesis of SnO_2 nanoparticles with better control of the microstructure using cost-effective techniques still remains a future challenge.

* Corresponding author. Tel.: +86 27 87557447; fax: +86 27 87545167.
E-mail address: huan@mail.hust.edu.cn (D. Zhou).

0272-8842/$34.00
doi:10.1016/j.ceramint.2008.04.010

Recently, the polyacrylamide gel has been demonstrated to be an efficient and cost-effective tool for easy synthesis of ultrafine oxide powders [21,22]. However, there are few reports about the synthesis of SnO_2 nanoparticles with this method. In this context, the polyacrylamide gel was introduced into the solution of Sn^{4+} as a temporary barrier, which was expected to inhibit the aggregation of nanoparticles. The microstructure of the as-synthesized nanoparticles was investigated and their potential for gas detection was demonstrated.

2. Experimental

2.1. Preparation of SnO_2 nanoparticles

The synthesis of SnO_2 nanoparticles with the aid of polyacrylamide gel can be described as a ''solution–gelation–combustion'' route. Acrylamide (AM) and *N*, *N*′-methylene-bisacrylamide (MBAM) were used as the reactive organic monomers. Ammonium persulfate (APS) was used as the initiator for the free-radical polymerization of the monomers. Firstly, AM, MBAM and APS were mixed together with the aqueous solution of Sn^{4+} obtained by dissolving $SnCl_4{\cdot}5H_2O$ in de-ionized water. The quantities of AM and $SnCl_4{\cdot}5H_2O$ per 500 mL of the mixed solution were both typically 40 g and APS 1.3 g, while the weight ratio of MBAM:AM varied from 1:100 to 1:10. Then, the solution was heated until an elastic hydrogel was rapidly obtained at about 70 °C. Finally, the hydrogel was directly calcined at temperatures of 600–1100 °C in air for 1 h, resulting in a heap of fine SnO_2 powders.

2.2. Formation of thick-film sensors

The sensor samples were fabricated by standard screen-printing thick-film technology. SnO_2 nanoparticles synthesized at 600 °C were slightly ground and mixed with terpineol-based vehicle consisting of ethyl cellulose and dibutyl phthalate (DBP) to form a viscous paste. A small amount of tin powders and glass frit were added in order to improve the film strength and the adhesion to the substrate. The paste was printed on planar 96%-alumina ceramics substrates. Each substrate was previously provided with interdigited Ag–Pd electrode. The films were then dried at 120 °C for 0.5 h and fired in air at 700 °C for 1 h.

2.3. Characterization

The xerogel samples after drying at 110 °C in air for 12 h were subjected to thermogravimetric analysis (TGA) using a thermal analyzer (STA 490C, NETZSCH, Germany) at a heating rate of 10 °C/min in static air. The phase purity and crystal structure of the particles were identified by X-ray powder diffraction (XRD) analysis with a diffractometer (X'Pert pro, PANalytical B V, Holland) using Cu Kα radiation (λ = 1.5418 Å). Morphology of the materials was observed by scanning electron microscope (SEM) (Sirion 200, FEI, Holland).

The gas-sensing response of the sensors was characterized by a gas-sensing characterization instrumentation (QMCS-I, HUST, China) where the sensor samples were mounted over the test-board in a chamber of 0.7 L volume with controlled temperature and humidity. The static method was used for sensing response and the gas concentration was determined by the volume ratio (within the test chamber). Note that the sensor sample was connected in series with a signal resistor (R_o). The sensor resistance could be calculated from the output voltage (V_o) of the signal resistor which was continuously recorded when the sensor was upon gas exposure. The gas response sensitivity (S) is defined as the ratio R_a/R_g, where R_a is the sensor resistance in clean air and R_g is the resistance when sensing responses to the test gas.

3. Results and discussion

3.1. Polymerization reaction

The monofunctional AM $CH_2{=}CHCONH_2$ and difunctional MBAM $(CH_2{=}CHCONH_2)_2CH_2$ are both olefinic monomers, and their polymerization could be initiated by free radicals offered by APS $(NH_4)_2S_2O_8$ and proceeds through chain initiation, chain propagation and chain termination [23,24]. Fig. 1 shows the free-radical polymerization of AM initiated by APS, which is thermally unstable and decompose into free-radical $SO_4^{\bullet -}$, carrying one unpaired electron with it. The free-radical $SO_4^{\bullet -}$ can attack the double bond in AM molecule, and add AM molecule to itself. While so adding, the free-radical site is simultaneously transferred from itself to AM unit. In the propagation steps, the radical site at the first AM unit attacks the double bond of a fresh AM molecule, resulting in the linking up of the second monomer unit to the first and transfer of the radical site from the first AM unit to the second. As more and more AM units are added, the length of the polymer chains increases continuously and the chains grow rapidly.

It can be seen that the polymerization of AM only results in a linear polymer. Therefore, a few quantities of difunctional MBAM consisting of two acrylamide units were added as a cross-linker. It can link the two growing linear chains and finally leads to the formation of polyacrylamide gel with a three-dimensional tangled network structure (Fig. 2). Due to the steric entrapment effect of the polyacrylamide gel, the

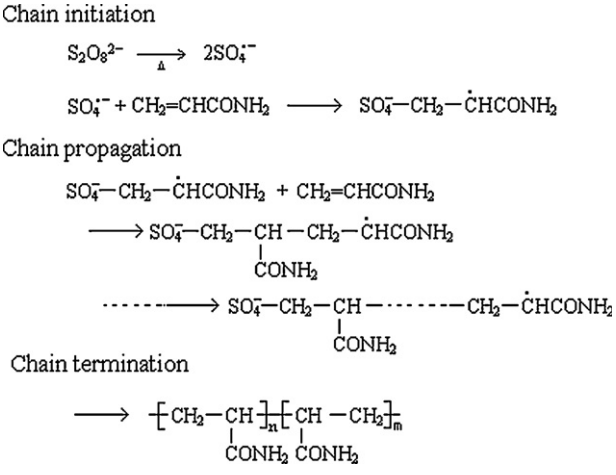

Fig. 1. Free-radical polymerization of AM.

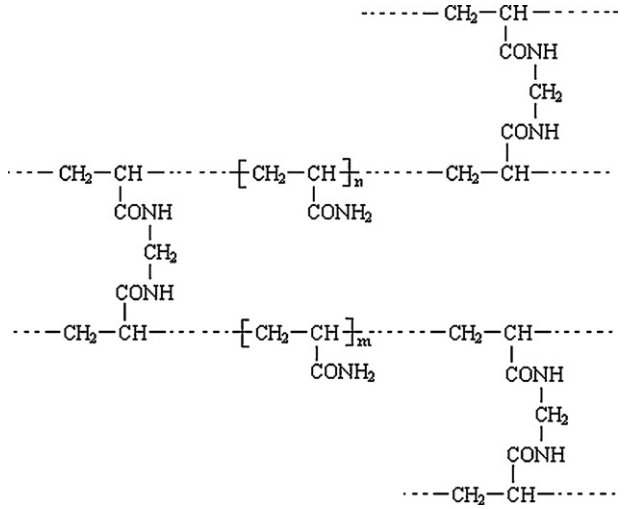

Fig. 2. Molecular structure of the polyacrylamide gel.

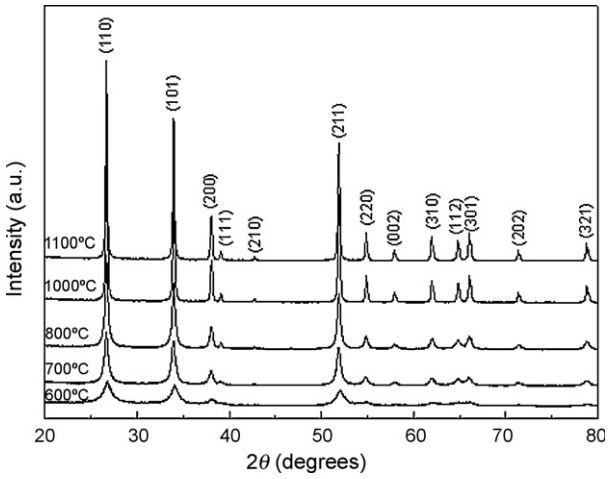

Fig. 4. XRD patterns of powders synthesized at various temperatures.

movement of Sn^{4+} in the aqueous solution was limited. With the aid of the 3D cross-linked polymer network as a temporary barrier, the chance of SnO_2 molecule aggregation in the calcination process is expected to be reduced, which helps to obtain SnO_2 nanoparticles without serious agglomeration.

3.2. Pyrolysis of the gel

Fig. 3 shows the thermogravimetric and differential thermogravimetric (TG–DTG) curves of the xerogel. Below temperatures of about 220 °C, polyacrylamides are generally thermally stable and undergo very little physical change. The slight weight loss was probably due to absorbed water from the environment and other volatile impurities [25]. The decomposition of the polyacrylamide gel occurred mainly in the temperature range of 220–600 °C and could be divided into three stages, which was in good agreement with the pyrolysis of neat gel based on methacrylamide (MAM) and MBAM reported by Janney et al. [26]. In the first stage approximately from 220 to 330 °C, the weight loss was about 18.1%. It has been shown that the weight loss at this stage may be ascribed to the release of water, ammonia, and small quantities of carbon dioxide as byproducts of imidization reactions occur via the

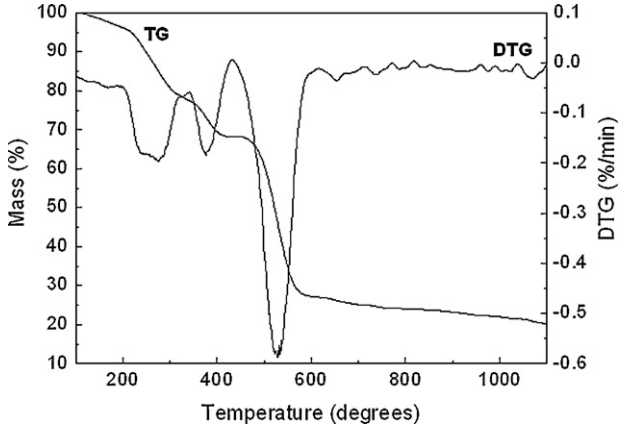

Fig. 3. TG–DTG curves of the xerogel.

pendant amide groups [27]. The weight loss of 9.8% in the second stage of 330–430 °C might be characterized by the breakdown of imides and main chains. In the third stage of 430–600 °C, the majority of the weight loss about 41% might be associated with the burnout of the carbon. No obvious weight loss was observed at higher temperatures, indicating that the calcination temperature above 600 °C was necessary for the removal of organic polymers.

3.3. Microstructure analysis

The XRD patterns of powders synthesized at various temperatures of 600–1100 °C are shown in Fig. 4. All the peaks were well consistent with JCPDS 21-1250 and no characteristic peaks of impurities were observed, which confirmed the samples as a pure tetragonal rutile crystalline SnO_2. It can be seen that the XRD peaks of the SnO_2 particles synthesized below 800 °C were broadened. With the Scherrer equation using full width at half-maximum of (1 1 0), (1 0 1) and (2 0 0) peaks, the average grain sizes of SnO_2 nanoparticles synthesized at 600, 700 and 800 °C were calculated to be 8.1, 19.2 and 27.9 nm, respectively. For the particles synthesized at higher calcination temperatures, XRD peaks became sharper without obvious extension in width. It can be concluded that the grain size and crystallinity increased with the calcination temperature in the range of 600–1100 °C.

Fig. 5 shows the SEM images of SnO_2 nanoparticles with different magnification. The 3D network of polyacrylamide gel decomposed during calcination process, leaving tin oxide particles in the form of a loosely held network, as shown in Fig. 5(a)–(c) provide closer view of an individual structure made up of sphere-like uniform nanoparticles agglomerated in thin platelets. It was obvious from Fig. 5(c) that the size of the particles was about 20–30 nm, which fitted in well with the values calculated from XRD patterns by the Scherrer equation.

The above results were based on the SnO_2 nanoparticles synthesized when the weight ratio of MBAM to AM was 1:25. Similar microstructure results were observed for other ratio values from 1:100 to 1:10. Although the gelation speed and gel

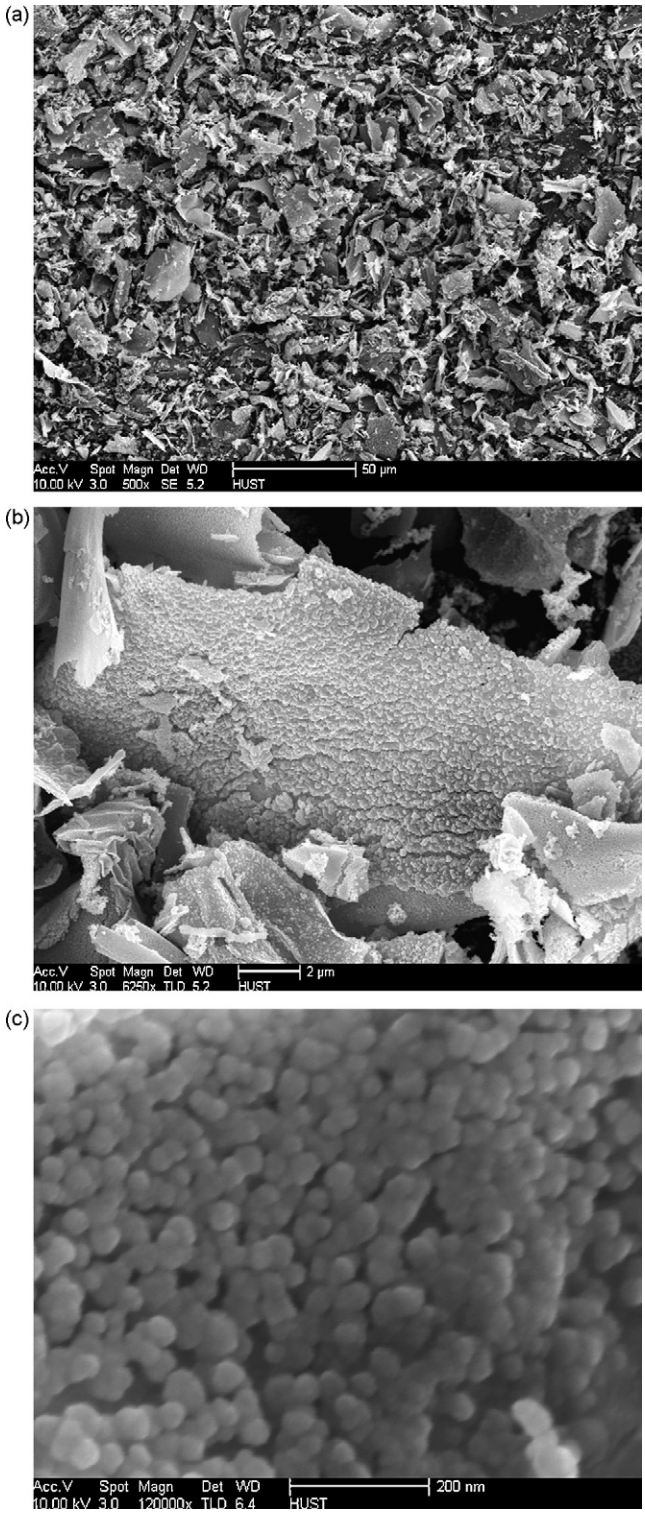

Fig. 5. SEM images of SnO_2 nanoparticles with different magnification (synthesized at 800 °C).

strength increased with the MBAM/AM weight ratio, the average grain sizes of SnO_2 nanoparticles were in the same range when synthesized at the same temperatures. This probably means that the grain size is actually determined more by the calcination temperature than by the gel properties [28]. Not much is known about the control of the powder morphology through that of the gel properties, and further investigations are needed.

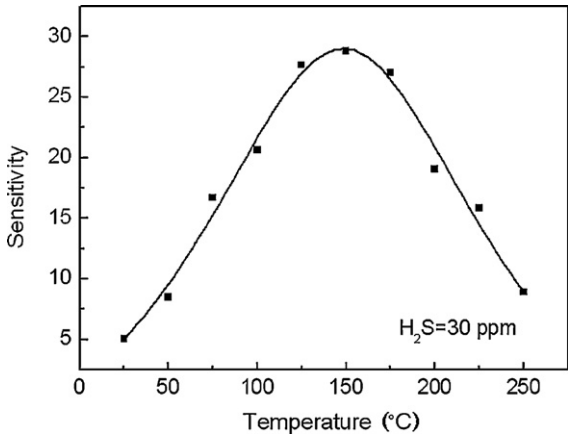

Fig. 6. Response sensitivity to 30 ppm of H_2S gas at different operation temperatures.

3.4. Sensing response properties

Responses of the thick-film sensor samples upon gas exposure at different temperatures from room temperature (25 °C) to 250 °C were tested in order to optimize the detection temperature. Corresponding response sensitivities toward 30 ppm of H_2S at these temperatures were calculated and plotted in Fig. 6. It can be seen that the thick-film sensor showed response to 30 ppm H_2S at 25 °C, and the response sensitivity increased with the temperature, having a maximum of around 28.8 at 150 °C, and then decreased with further rise in temperature. This good response performance might be associated with the structural and electrical stabilities of SnO_2 nanoparticles that are beneficial to the development of porous microstructure with uniform nanoparticles in the thick film, thus providing greater active surface area and gas penetration.

The exposures to low concentrations (0.7–100 ppm) of H_2S when operated at 150 °C were also conducted. The whole testing-cycle time was set to be 500 s. The response sensitivity

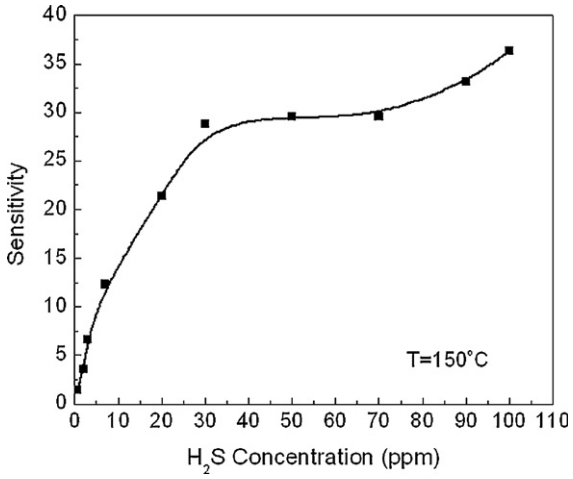

Fig. 7. Response sensitivity to different concentrations of H_2S gas at the optimal temperature.

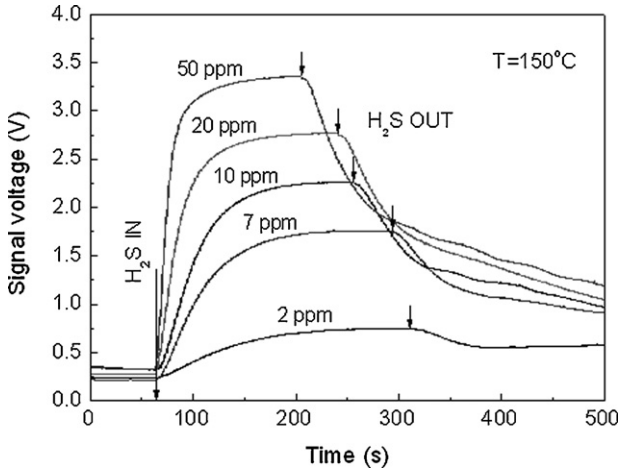

Fig. 8. Response curves to different concentrations of H_2S gas at the optimal temperature.

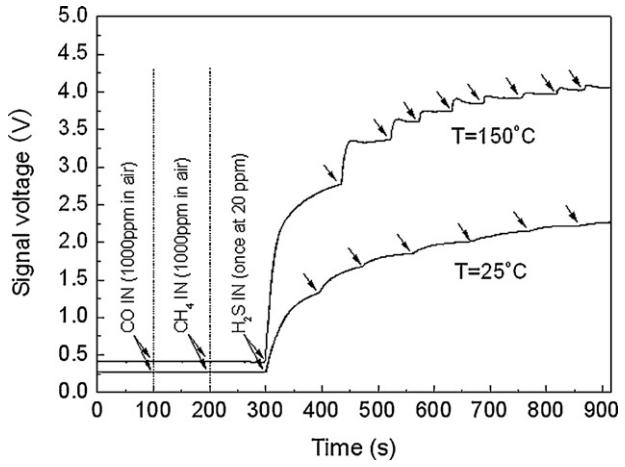

Fig. 9. Response curves of the thick-film sensor to various test gases.

as a function of the gas concentration was plotted in Fig. 7 and some response curves were given in Fig. 8. Both the sensitivity and speed of the response increased monotonically with the concentration of H_2S gas, confirming the applicability of pure SnO_2 nanoparticles in the detection of ppm-level concentrations of H_2S gas at relatively low temperatures. When operated at 150 °C, the responses time (time to rise to 90% of final value of the sensitivity) of the sensors for H_2S gas above 20 ppm were all within 50 s. The sensors were also sensitive to trace amount (below 2 ppm) of H_2S gas at 150 °C. Minor deviation of the initial signal voltage occurred due to a couple of repeated cycles.

The selectivity of thick-film sensors was also examined. Fig. 9 shows the response curves of the sensor upon sequential exposure to CO, CH_4 and H_2S (continuous injection once at 20 ppm). Obviously, when operated at the optimal detection temperature of 150 °C or at room temperature, the sensors were highly selective to low concentration of H_2S without serious interference from CO and CH_4. Although the responses of the sensor to H_2S dropped after several times of injection due to the saturation of gas adsorption, the possibility for the detection of low concentrations of H_2S at relatively low temperatures with the as-synthesized SnO_2 nanoparticles without specific additives had been demonstrated.

4. Conclusions

The polyacrylamide gel was successfully utilized to synthesize tin oxide nanoparticles. The solution of Sn^{4+} was gelled due to the copolymerization of AM and MBAM. Direct combustion of the gel resulted in sphere-like uniform nanoparticles slightly agglomerated in thin platelets. The average grain sizes of SnO_2 nanoparticles synthesized at 600, 700 and 800 °C were calculated to be 8.1, 19.2 and 27.9 nm respectively. Thick-film sensors based on the as-synthesized SnO_2 nanoparticles without specific additives were sensitive and selective to low concentrations of H_2S both at the optimal detection temperature of 150 °C and at room temperature, which are highly attractive for the practical application in H_2S gas detection.

Acknowledgement

This work was financially supported by Specialized Research Fund for the Doctoral Program of Higher Education of China (20070487182).

References

[1] N. Yamazoe, New approaches for improving semiconductor gas sensors, Sens. Actuators B: Chem. 5 (1991) 7–19.
[2] N. Yamazoe, G. Sakai, K. Shimanoe, Oxide semiconductor gas sensors, Catal. Surv. Asia 7 (2003) 63–75.
[3] S.P. Gong, H. Liu, D.X. Zhou, Progress in nanophase tin oxide gas sensors and gas-sensitive array, J. Inorg. Mater. 21 (2006) 521–526.
[4] A. Salchi, A highly sensitive selfheated SnO_2 carbon monoxide sensor, Sens. Actuators B: Chem. 96 (2003) 88–93.
[5] L.A. Patil, D.R. Patil, Heterocontact type CuO-modified SnO_2 sensor for the detection of a ppm level H_2S gas at room temperature, Sens. Actuators B 120 (2006) 316–323.
[6] C.N. Xu, J. Tamaki, N. Miura, N. Yamazoe, Correlations between gas sensitivity and crystallite size in porous SnO_2-based sensors, Chem. Lett. 219 (1990) 441–444.
[7] C.N. Xu, J. Tamaki, N. Miura, N. Yamazoe, Grain size effect on gas sensitivity of porous SnO_2-based elements, Sens. Actuators B: Chem. 3 (1991) 147–155.
[8] A.M. Gaskov, M.N. Rumyantseva, Nature of gas sensitivity in nanocrystalline metal oxides, Russ. J. Appl. Chem. 74 (2001) 440–444.
[9] E. Comini, Metal oxide nano-crystal for gas sensing, Anal. Chim. Acta 568 (2006) 28–40.
[10] A. Rothschild, Y. Komem, The effect of grain size on the sensitivity of nanocrystalline metal-oxide gas sensors, J. Appl. Phys. 95 (2004) 6374–6380.
[11] A. Dieguez, A.R. Rodriguez, J.R. Morante, U. Weimar, M.S. Berberich, W. Göpel, Morphological analysis of nanocrystalline SnO_2 for gas sensor application, Sens. Actuators B 31 (1996) 1–8.
[12] K. Kalyanasundaram, P.I. Gouma, Processing and characterization of nanostructured metal oxides for gas sensing application, IEEJ Trans. SM 126 (2006) 560–567.
[13] A. Chandra Bose, P. Thangadurai, S. Ramasamy, Grain size dependent electrical studies on nanocrystalline SnO_2, Mater. Chem. Phys. 95 (2006) 72–78.
[14] O. Acarbas, E. Suvaci, A. Dogan, Preparation of nanosized tin oxide (SnO_2) powder by homogeneous precipitation, Ceram. Int. 33 (2007) 537–542.
[15] M. Epifani, E. Comini, R. Diaz, J. Arbiol, P. Sciciliano, G. Sberveglieri, J.R. Morante, Oxide nanopowders from the low-temperature processing of

metal oxide sols and their application as gas-sensing materials, Sens. Actuators B 118 (2006) 105–109.
[16] S. Fujihara, T. Maeda, H. Ohgi, E. Hosono, H. Imai, S.H. Kim, Hydrothermal routes to prepare nanocrystalline mesoporous SnO_2 having high thermal stability, Langmuir 20 (2004) 6476–6481.
[17] R.S. Niranjan, Y.K. Hwang, D.K. Kim, S.H. Jhung, J.S. Chang, I.S. Mulla, Nanostructured tin oxide: synthesis and gas-sensing properties, Mater. Chem. Phys. 92 (2005) 384–388.
[18] G. Williams, G.S.V. Coles, The gas-sensing potential of nanocrystalline tin oxide produced by a laser ablation technique, MRS Bull. 24 (1999) 25–29.
[19] O.K. Tan, W. Cao, Y. Hu, W. Zhu, Nano-structured oxide semiconductor materials for gas-sensing application, Ceram. Int. 30 (2004) 1127–1133.
[20] M.I. Baraton, L. Merhari, Nanoparticles-based chemical gas sensors for outdoor air quality monitoring microstations Mater, Sci. Eng. B 112 (2004) 206–213.
[21] A. Douy, Polyacrylamide gel: an efficient tool for easy synthesis of multicomponent oxide precursors of ceramics and glasses, Int. J. Inorg. Mater. 3 (2001) 699–707.
[22] A. Calleja, X. Casas, I.G. Serradilla, M. Segarra, A. Sin, P. Odier, F. Espiell, Up-scaling of superconductor powders by the acrylamide polymerization method, Physica C 372–376 (2002) 1115–1118.
[23] J.M.G. Cowie, Polymers: Chemistry and Physics of Modern Materials, 2nd ed., Chapman and Hall, New York, 1991.
[24] V.R. Gowariker, N.V. Viswanathan, S. Jayadev, Polymer Science, John Wiley & Sons, New York, 1986.
[25] M.J. Caulfield, G.G. Qiao, D.H. Solomon, Some aspects of the properties and degradation of polyacrylamides, Chem. Rev. 102 (2002) 3067–3083.
[26] M.A. Janney, O.O. Omatete, C.A. Walls, S.D. Num, R.J. Ogle, G. Westmoreland, Development of low-toxicity gelcasting systems, J. Am. Ceram. Soc. 81 (1998) 581–591.
[27] J.D. Van Dyke, K.L. Kasperski, Thermogravimetric study of polyacrylamide with evolved gas analysis, J. Polym. Sci. Pol. Chem. 31 (1993) 1807–1823.
[28] A. Sin, P. Odier, Gelation by acrylamide, a quasi-universal medium for the synthesis of fine oxide powders for electroceramic applications, Adv. Mater. 12 (2000) 649–652.